Solar Energy Materials & Solar Cells 219 (2021) 110815

Contents lists available at ScienceDirect

Solar Energy Materials and Solar Cells

journal homepage: http://www.elsevier.com/locate/solmat

Optimization of front SiN_x/ITO stacks for high-efficiency two-side contacted c-Si solar cells with co-annealed front and rear passivating contacts

Frank Meyer [a,*], Arnaud Savoy [a], Juan J. Diaz Leon [b], Marc Persoz [a], Xavier Niquille [a], Christophe Allebé [b], Sylvain Nicolay [b], Franz-Josef Haug [a], Andrea Ingenito [a,b], Christophe Ballif [a,b]

[a] Ecole Polytechnique Fédérale de Lausanne (EPFL), Institute of Microengineering (IMT), Photovoltaics and Thin Film Electronics Laboratory, Rue de la Maladière 71b, 2002, Neuchâtel, Switzerland
[b] CSEM PV-Center, Jaquet-Droz 1, 2002, Neuchâtel, Switzerland

ARTICLE INFO

Keywords:
Passivating contacts
Silicon solar cells
Hydrogenation
Sputtering
Indium-tin-oxide (ITO)

ABSTRACT

In this contribution, we present an electron selective passivating contact metallised with a low temperature process to target front side applications in crystalline silicon (c-Si) solar cells. In addition to an interfacial silicon oxide (SiO_x) and an in-situ phosphorous doped micro-crystalline silicon (μc-Si(n)) layer, it comprises an ultra-thin indium tin oxide (ITO) layer of 15 nm for lateral conductivity and a hydrogen rich silicon nitride (SiN_x:H) layer which serves as hydrogen (H) reservoir and as anti-reflection coating. We use one single thermal treatment for 30 min at 350 °C to sinter the screen-printed paste, to recover sputtering damage induced during ITO deposition, and to diffuse hydrogen from the SiN_x:H layer towards the c-Si/SiO_x interface where it passivates interfacial defects.

Applied to symmetrically processed textured samples, we find implied open-circuit voltage (iV_{OC}) > 728 mV for optimal ITO thickness of 15 nm and annealing temperatures of 350 °C. The developed stack was applied on the front textured side of co-annealed (800 °C) p-type c-Si solar cells in combination with a tunnel oxide hole selective passivating contact on the rear side. We demonstrate solar cells with fill factor (FF) up to 81.9% and an open-circuit voltage (V_{OC}) up to 719 mV. With a short-circuit current density (J_{SC}) of 38.6 mA/cm^2, we obtain a final cell efficiency to 22.8%. We find that the annealing of the SiN_x:H/ITO stack strongly increases the ITO free carrier density penalizing the solar cell spectral response at high wavelengths.

1. Introduction

Recombination at the direct metal-silicon contact is the main efficiency limiting factor for industrial as well as laboratory scale c-Si solar cells, mainly through suboptimal V_{OC} [1–3]. Passivating contacts mitigate contact recombination losses by separating the metal electrodes from the active semiconductor. For example, silicon heterojunction (SHJ) solar cells can reach conversion efficiency up to 26.7% when combined in an interdigitated back contact design by passivating the wafer surface with a layer of hydrogen-rich amorphous silicon [4]. One of the main drawbacks of SHJ is their incompatibility with currently established PV manufacturing processes. Alternatively, tunnel oxide passivating contacts have enabled high conversion efficiency (>25.5%), while being potentially compatible with industrial processes at elevated temperatures [5,6]. These passivating contacts generally consist of a thin (1.2–3.6 nm) SiO_x layer on which a doped poly-silicon layer is deposited. The poly-silicon is then crystallized by annealing at temperatures >800 °C, forming at the same time a buried doped region below the Si/SiO_x interface [7–15]. In most cases, a hydrogenation step is performed to reduce the electronic defects at this interface, and thus to reach high V_{OC} values [16–18]. One solution for the hydrogenation consists in depositing a hydrogen rich silicon-nitride SiN_x:H layer followed by a thermal treatment to diffuse H from the SiN_x:H to the Si/SiO_x interface [17–19].

On the short-term, passivating contacts are frontrunners to upgrade current industrial p-PERC and n-PERT solar cell technologies. Recently,

* Corresponding author.
E-mail address: frank.meyer@epfl.ch (F. Meyer).

https://doi.org/10.1016/j.solmat.2020.110815
Received 5 June 2020; Received in revised form 18 September 2020; Accepted 19 September 2020
Available online 29 September 2020

Trina solar has demonstrated an upgraded n-PERT process with conversion efficiency up to 24.6% [20]. Despite this impressive result, to keep on increasing solar cell conversion efficiency, passivating contacts have to be employed also on the front side of the solar cell, in order to mitigate front side recombination losses [21]. In this respect, a simple approach consists in using a thin poly-Si layer combined with a transparent conductive oxide (TCO) providing lateral conductivity [12–15]. However, if using SiN_x:H for hydrogenation, it needs to be removed before applying the TCO. Moreover, passivating contacts suffer from higher sputtering damage compared to conventional silicon heterojunctions, especially when applied on textured surfaces. Damage can be partially recovered by a subsequent thermal treatment [22,23].

In this contribution, we present passivating contacts covered with a SiN_x:H/ITO stack, and we demonstrate a thermal treatment that provides at the same time hydrogenation of the c-Si/SiO_x interface as well as curing of the induced sputtering damage. In the presented approach, the SiN_x:H is deposited as final layer after the annealing of the poly-Si layer, the sputtering of the ITO, and the screen printing of the Ag-grid. By optimizing the ITO thickness and thermal treatment, we demonstrate low-temperature contacted poly-Si layers with implied V_{OC} (iV_{OC}) up to 730 mV. This result indicates that our SiN_x:H/ITO stack is a valid solution to recover sputter-induced damage and to provide hydrogenation of the c-Si/SiO_x interface. Additionally, this contact design provides a process simplification as the SiN_x:H does not need to be etched. Instead, it contributes to the anti-refection coating (ARC), enabling the use of thinner ITO and thus allowing for a reduction of manufacturing costs. The developed passivating contact and metallisation scheme was applied to the textured front side of p-type c-Si solar cells in combination with a full-area p-type passivating contact on the rear side. Solar cell conversion efficiency up to 22.8%, with 15 nm thick front ITO layer, were fabricated.

2. Experimental

Symmetrical test structures were fabricated on <100> oriented n-type float zone (FZ) wafers with thickness of 180 μm and resistivity of 2 Ω cm^2 on which standard wet cleaning and texturing was performed. After the growth of a thin (1–2 nm) SiO_x by UV-Ozone (UV–O_3) in ambient air [24–26], an in-situ phosphorous doped μc-Si(n) layer was deposited by plasma enhanced chemical vapour deposition (PECVD) at 200 °C on both sides of the wafer, followed by an annealing in inert atmosphere at 850 °C in a tube furnace. After annealing, a set of samples was hydrogenated by depositing by PECVD at 250 °C a 70–80 nm thick SiN_x:H layer followed by annealing at 450 °C for 30 min. After stripping of this SiN_x:H layer in hydrofluoric acid (HF), ITO with nominal thicknesses of 15, 30 or 60 nm were sputtered. The process is illustrated in Fig. 1a (i.e. standard process). A second set of samples was processed by sputtering of ITO with different thicknesses directly on the annealed SiO_x/μc-Si(n) stack, followed by the same SiN_x:H deposition than the one used for the first set of samples. The process is illustrated in Fig. 1b. Both sets of samples were finally annealed at different temperatures on a hotplate in air. For the first set of samples (standard process), a post-annealing of 5 min at different peak temperature was used to cure sputtering damage. For the second set, a thermal treatment of 30 min was used to allow the H released from the SiN_x:H to diffuse through the ITO/μc-Si(n) stack (H-through process). The minority carrier lifetime (τ_{eff}) was measured at 10^{15} cm^{-3} minority carrier density (MCD) for all samples by photo-conductance decay using a Sinton WCT-120, and iV_{OC} was computed [27–29]. Contact resistivity (ρ_c) and sheet resistance (R_{sheet}) were assessed by means of transmission line measurements (TLM) [30,31]. For the sample preparation, symmetrical n-type textured (txt) wafer with tube annealed μc-Si(n) layer were prepared in order to compare the performance of standard and H-through processes. According to the first, wafers were hydrogenated by annealing of a SiN_x:H at 450 °C for 30min, after stripping of the SiN_x:H in HF, ITO layers of the three different thicknesses were sputtered on the full-area. The Ag pads were deposited and the wafers were cleaved close to TLM structure to avoid lateral current spreading during the measurement. According with the H-through process, SiN_x:H was deposited on top of the TLM structure (ITO on full area + Ag pads). The samples were then cured in two different ambient (N_2 and air) for 30 min for H-through process and 5 min for the standard process. Moreover, the carrier concentration (N_{Hall}) and the Hall mobility (μ_{Hall}) were measured by Hall-Effect, using a van der Pauw configuration with square samples [32]. For these measurements, the wafer was isolated from the ITO layer by a thick (~30 nm) thermal oxide on which the ITO and SiN_x:H/ITO layers were deposited directly. The corners of the structure were masked during the SiN_x:H deposition to ensure a good electrical contact between the probes and

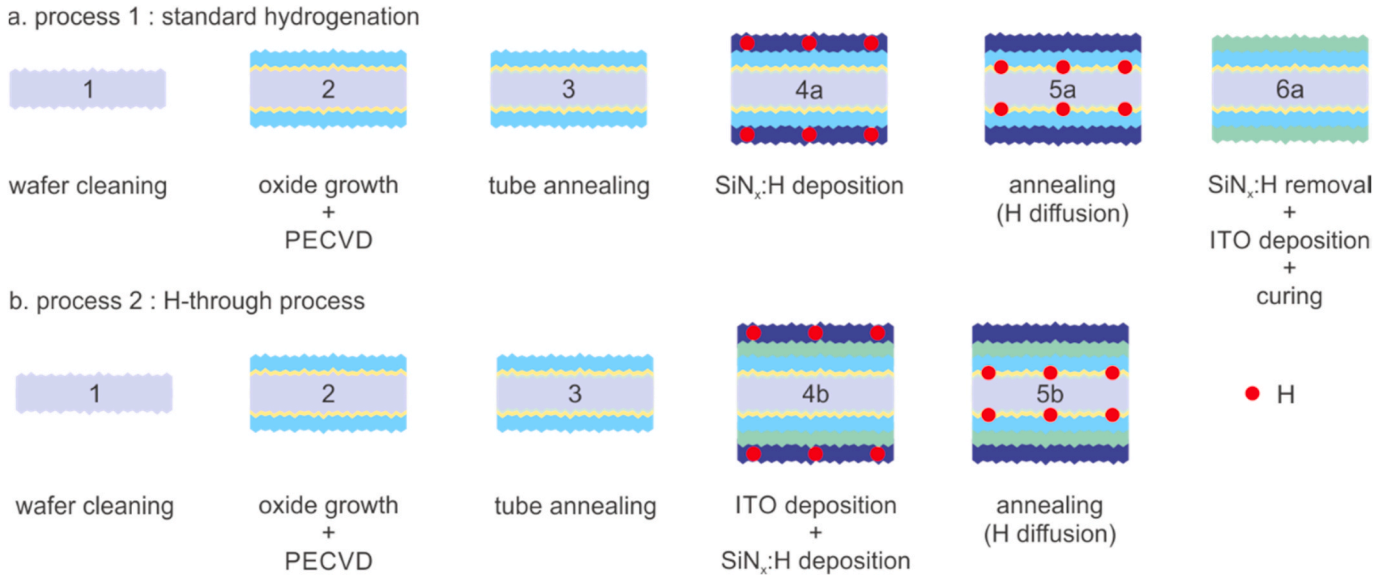

Fig. 1. – a. Standard hydrogenation process b. H-through process 1. Cleaning of the n-type wafer 2. Oxide growth by exposure to UV-O_3 and deposition of the μc-Si (n) contact by PECVD 3. Annealing in a tube furnace at 800 °C and creation of the buried junction 4a. Deposition of the SiN_x:H by PECVD 5a. Diffusion of H by hot plate annealing at 450 °C 6a. Removal of the SiN_x:H layer, sputtering of the ITO layer (15, 30 or 60 nm) and curing at different temperature to recover the sputtering damage 4b. ITO deposition by sputtering and SiN_x:H deposition by PECVD 5b. Diffusion of H and curing of the sputtering damage.

the sample. Furthermore, absorption of the single ITO layer and of the SiN_x:H/ITO stack were measured on glass substrate using a spectrophotometer (PerkinElmer, lambda 950).

Finally, solar cells with full-area passivating contacts were processed. To this end, we used front side textured FZ p-type <100> oriented wafers with a thickness of 190 μm and resistivity of 2 Ω cm^2. After standard cleaning, a thin oxide was grown by exposure to UV-O_3 as explained above. In-situ doped poly-silicon-based electron (μc-Si(n)) and hole selective (SiC_x(p)) layers were deposited by PECVD, followed by annealing at 850 °C in a tube furnace. Subsequently, a 15 nm-thick ITO was sputtered through a mask to define the 2 cm × 2 cm cell area on the front side and an Ag-grid was screen-printed. The metallisation fraction of the Ag-grid was 2.35% and we used a low temperature paste, typically used for SHJ solar cells, dried at 210 °C for 30 min. Finally, a 50–55 nm thick SiN_x:H layer was deposited at the front side of the cells and a 70–80 nm thick layer was deposited at the rear. The SiN_x:H thickness of the front layer is a bit thinner to ensure a good ARC with the ITO deposited before. The real refractive index of the SiN_x:H was 2.1 at wavelength of 633 nm. The PECVD deposition was followed by annealing in N_2 at temperature of 350 °C for 30 min. The SiN_x:H was etched from the rear side only, and an ITO/Ag stack was sputtered through the same mask aligned with the front structure. The cell structure is illustrated in Fig. 2. Current - voltage (I–V) characteristics were measured at 25 °C with a source meter (Keithley, 2601A) by using an AAA Wacom sun simulator calibrated with a reference cell. The region outside of the cell was masked during the I–V measurements. Suns-V_{OC} were measured with Sinton WCT-120 instrument [28] and the EQE of the cell was measured between the fingers.

3. Results

3.1. Surface passivation

To demonstrate the feasibility of the H diffusion through the ITO layer, we prepared symmetrical samples with SiN_x:H/ITO stacks and applied different annealing temperatures. Fig. 3a, b and c show, respectively, the minority carrier lifetime, iV_{OC} values, and recombination current density (J_0) obtained for annealing in air ambient. Compared to the values directly after ITO sputtering, annealing at 300 °C provides a slight increase in lifetime and iV_{OC} and a decrease of J_0. This suggests that this temperature is insufficient to provide enough H to the c-Si/SiO_x interface and/or to fully recover from sputtering damage. However, if we suppose that no H diffusion occurs at 300 °C, this temperature may be enough to recover the sputtering damage since the lifetime, iV_{OC} and J_0 values are close to the ones prior the ITO deposition. Increasing the temperature to 350 °C, resulted in a strong boost in lifetime and iV_{OC} and a strong decrease of J_0 for all ITO thicknesses shown. The highest lifetime (at injection level of 10^{15} cm^{-3}) of >4.5 ms and iV_{OC} up to 732 mV were reached for a 15 nm thick ITO film. At 400 °C, the lifetimes and iV_{OC} still slightly increased, with thinner ITO enabling higher passivation gains. Finally, at 450 °C, the iV_{OC} values decrease regardless of the ITO thickness. We interpret the result as follows: temperatures of 350 °C are required to provide a sufficient amount of H to passivate interfacial dangling bonds and partially recover from sputtering damage whereas at 450 °C a further recovery from sputtering damage is counterbalanced by H out-effusion from the c-Si/SiO_x interface. With respect to ITO thickness, we observe that thinner ITO layers yield higher lifetimes and iV_{OC} values, as they possibly facilitate H diffusion. From Fig. 3c, we note that J_0 continues to decrease even at 450 °C, suggesting that higher temperature provides more H to the c-Si/SiO_x interface. This trend is no followed by the lifetime and the iV_{OC} which decreases at temperature between 400-450 °C, we correlate this mismatch to a wafer bulk effect. In all cases, the values remain below the horizontal dashed lines that denote the lifetime and the iV_{OC} of a standard hydrogenation process before ITO deposition (step 5a in Fig. 1), indicating that none of the annealing processes can fully recover the sputtering damage and/or diffuse the same amount of H in the oxide layer. Generally, this value represents the upper limit for the iV_{OC} and is normally degraded after metallisation.

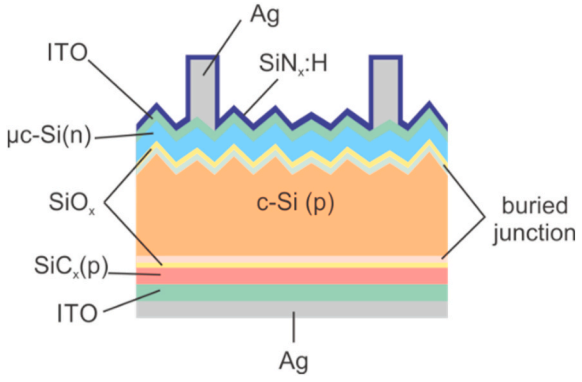

Fig. 2. Solar cell structure employing the H-through process on the front side.

However, the values for the lifetime and the iV_{OC} obtained after annealing for the H-through process (step 5b in Fig. 1) is always higher than the corresponding values obtained with the standard hydrogenation after deposition and curing of the ITO (step 6a in Fig. 1) shown in Fig. 4. Oppositely, the values for the J_0, except for the sample with 60 nm of ITO, are always below the values obtained with the standard hydrogenation for the equivalent process steps. In Fig. 4c, we note that the J_0 values start increasing between 350 and 400 °C which could indicate an easier loss of hydrogen as the samples are no longer capped with SiNx, thus counteracting the curing of the sputtering damage. We conclude that the H-through process can enable higher passivation either by still ensuring diffusion of H, avoiding its effusion and/or by a better recovering of the sputtering damage probably due to its longer annealing time. We also notice that for both sets of samples, the lifetime, iV_{OC} and J_0 values after ITO deposition are approximately constant, suggesting that most of the sputtering damage happens during the deposition of the first 15 nm whereas the longer processes of the thicker layers add none or only little additional damage.

3.2. Contact resistance

For our front contact design we have to take into account two contributions to the series resistance: (1) the lateral transport into the ITO, the passivating contacts and the wafer (2) the contact resistance that comprises the contact resistance between ITO layer, the Ag metallisation and the passivating contact. Due to the contribution of the wafer, it was not possible to isolate only the ITO contribution for lateral transport, the trends are only indicative.

Fig. 5a and b show respectively R_{sheet} and ρ_c deduced from the TLM measurements after curing in air. For the standard hydrogenation without any SiN_x:H capping on top of the ITO layer, R_{sheet}, stays <60 Ω/square for curing at 350 °C, but it degrades quickly to R_{sheet} >100 Ω/square for higher curing temperatures. Starting at 400 °C for 60 nm of ITO and starting at 350 °C for the two other ITO thicknesses, the TLM structures degrade after annealing. For these conditions, the TLM characteristic did no longer vary linearly with the pad distance which we attribute to Ag peeling, a critical degradation of the ITO, or possibly partial delamination of the film. Under these conditions, the R_{sheet} can exceed the one of the wafer. The ρ_c and R_{sheet} extracted for these temperatures are shown in Fig. 5, but they are meant to illustrate degradation of the ITO rather than real values. For the H-through process, R_{sheet} never exceeds the critical value of 100 Ω/square and stays below 70 Ω/square. The values of ρ_c in Fig. 5b show a more drastic behaviour as the critical value is already surpassed for curing temperature of 350 °C. In contrast, ρ_c of the H-through samples stays below 50 mΩ·cm^2 for curing at 350 °C and values above 100 mΩ·cm^2 are only observed for the

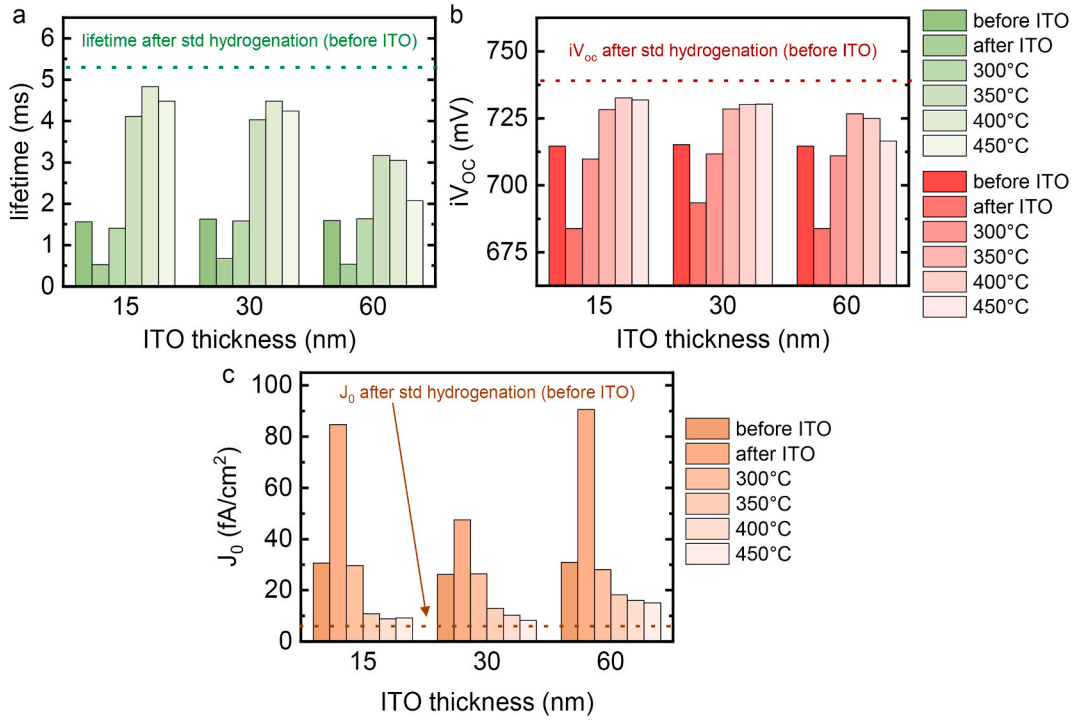

Fig. 3. – a. Minority carrier lifetime (ms) at injection level of 10^{15} cm^{-3} as a function of the ITO thickness (nm) for H-through process b. iV$_{oc}$ (mV) deduced from the lifetime in function of the ITO thickness (nm) for H-through process. c. J$_0$ (A/cm^2) as a function of the ITO thickness (nm) for H-through process. Samples in a, b and c were annealed in air ambient.

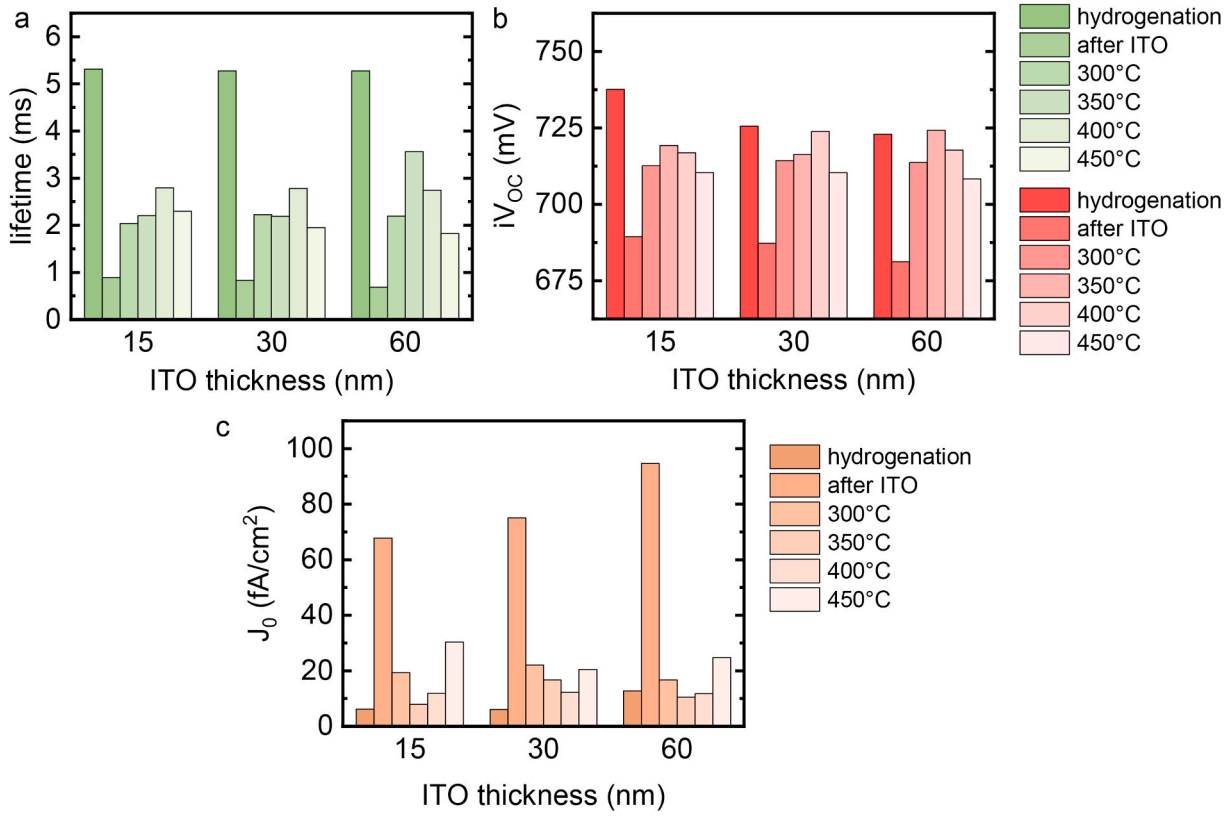

Fig. 4. - a. Minority carrier lifetime (ms) at injection level of 10^{15} cm^{-3} as a function of the ITO thickness (nm) for standard hydrogenation b. iV$_{oc}$ (mV) deduced from the lifetime in function of the ITO thickness (nm) for standard hydrogenation. c. J$_0$ (A/cm^2) as a function of the ITO thickness (nm) for standard hydrogenation. Samples in a, b and c were annealed in air ambient.

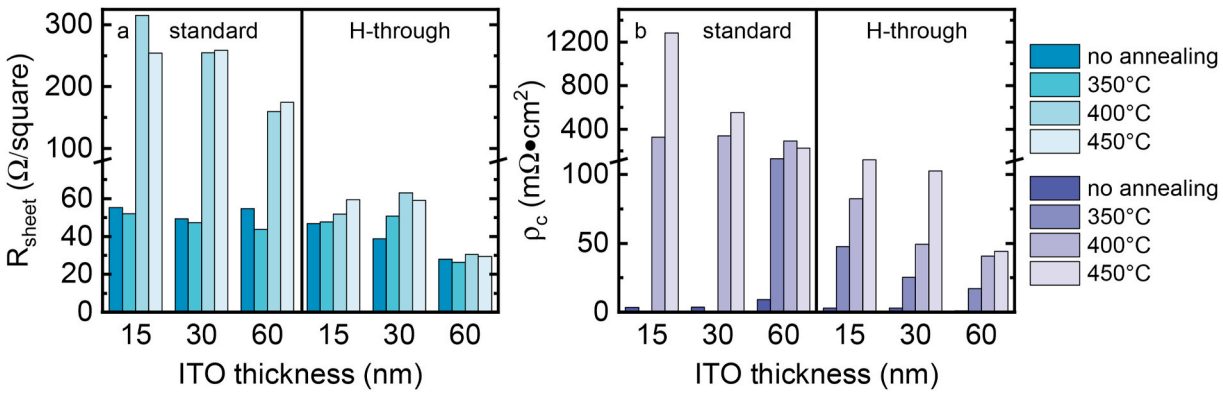

Fig. 5. - a. R_{sheet} (Ω/square) as a function of the ITO thickness (nm) for the H-through and standard hydrogenation process b. ρ_c (mΩ·cm^2) in function of the ITO thickness (nm) for H-through and standard hydrogenation process. Samples in a and b were annealed in air ambient.

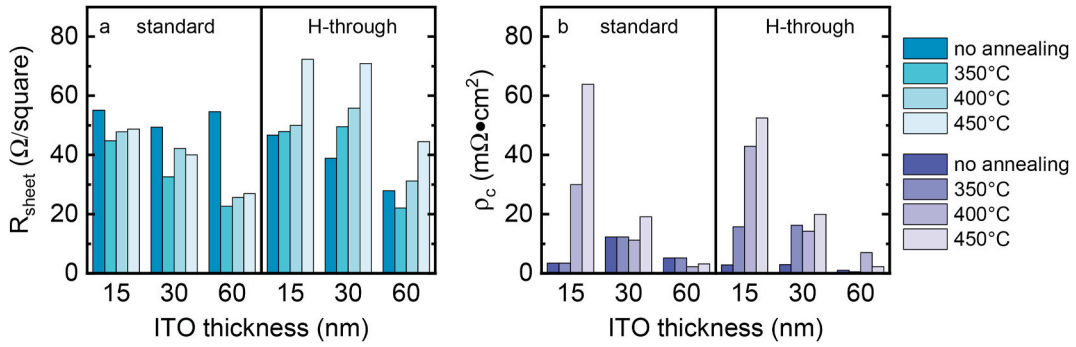

Fig. 6. - a. R_{sheet} (Ω/square) as a function of the ITO thickness (nm) for the H-through and standard hydrogenation process b. ρ_c (mΩ·cm^2) as a function of the ITO thickness (nm) for H-through and standard hydrogenation process. Samples in a and b were annealed in N_2 ambient.

15 nm thick ITO when cured at 450 °C.

Fig. 6a and b show respectively the R_{sheet} and the ρ_c after curing in N_2 ambient. In this case, the electrical properties of the ITO layer are preserved also for the standard hydrogenation as none of the R_{sheet} exceed 60 Ω/square. The H-through samples behave similarly for the low curing temperatures, only those cured at 450 °C show an increase. All of the ρ_c shown in Fig. 6b stay below 70 mΩ·cm^2, those of the H-through process are even below 55 mΩ·cm^2. For the standard samples we tentatively interpret the different behaviour of R_{sheet} in Figs. 5a and 6a by a loss of carrier density due to saturation of oxygen vacancies. For the H-through process the loss appears to be less pronounced presumably because the SiN_x:H capping layer protects the ITO layer. The behaviour of ρ_c in Figs. 5b and 6b corroborates this interpretation; as ρ_c is likely dominated by the Schottky contact between ITO and the metallisation [33], a loss of carrier density in the ITO will widen the tunnelling barrier and thus increase ρ_c.

3.3. Solar cell results

The TLM and QSSPC results of the previous sections suggest that an ITO thickness of 15 nm and an annealing temperature 350 °C promise to yield the best combination in terms of passivation as well as ρ_c and R_{sheet}. Accordingly, we processed solar cells by applying a full area SiN_x:H/ITO/μc-Si(n) contact on the textured front side and a full area Ag/ITO/SiC(p) on the planar rear side of a p-type wafer as shown in Fig. 2. The annealing time was fixed at 30 min to allow the H released from the SiN_x:H to diffuse through the ITO/μc-Si(n) stack as explained in the experimental part. The J-V characteristics deduced from the I–V measurements of the best cell obtained with the H-through process are shown in Fig. 7a. To understand the losses at the cell level, Suns-V_{OC} is also displayed on this graph. We measure V_{OC} of 719 mV and FF of 81.9%. We attributed the loss of V_{OC} to the rear contact since the iV_{OC} measured previously on symmetrical n-type txt samples is above 728 mV. A ρ_c of 16 mΩ·cm^2 with a metallisation fraction of 2.35% at the front side induces more than 3% losses in the FF which can explain the difference between the pseudo FF (pFF) and the measured FF of the cell. The rear side is not the limiting parameter in terms of FF since the metallisation covers the full area. However, the conversion efficiency is limited by a relatively low J_{SC} of 38.6 mA/cm^2. We compare in Fig. 7b the EQE of our best cell with a cell made with a standard hydrogenation process on the textured front side, using a 5 min post-curing in N_2 at 350 °C to recover from sputtering damage. We observe a decrease in the absorption in the near IR-region which we attribute to free carrier absorption in the ITO. Fig. 7c shows the mobility and the bulk carrier concentration measured by Hall-Effect after curing in N_2 ambient. In the case of a standard hydrogenation, the mobility and bulk concentration are constant for the three different curing temperatures since the oxygen vacancies are supposed to stay constant during the annealing in N_2 ambient. Moreover, we observe a decrease in mobility and an increase in bulk carrier concentration after the first curing whereas in the case of the H-through process, this behaviour is not observed. This is related to SiN_x:H deposition at 250 °C which can be correlated to an annealing in vacuum atmosphere at the same temperature. However, bulk carrier concentration still increases and the mobility still decreases with the annealing temperature. Already at 350 °C, the bulk carrier concentration is almost doubled compared to a standard process. The consequence of this increase can be observed in Fig. 7d where the free carrier absorption of the H-through samples layer systematically increases with the annealing temperature. We observed that absorption in the bandgap region is increased at the same time.

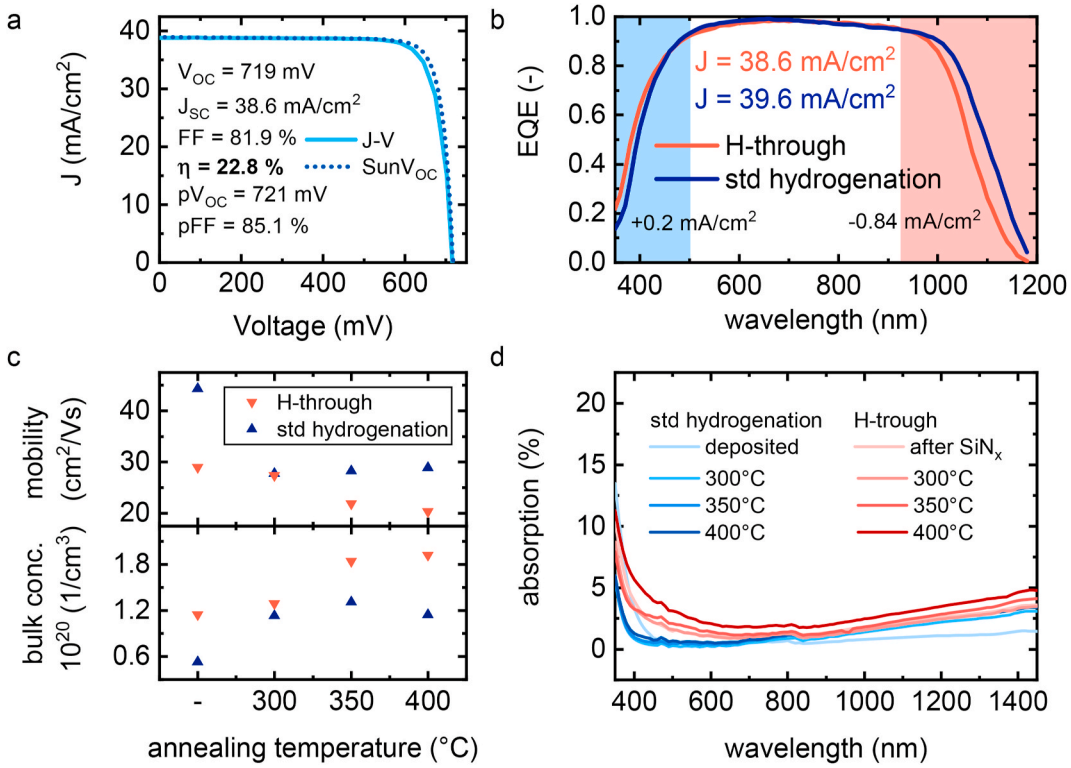

Fig. 7. – a. J-V characteristics and Suns -V_{OC} measurement of the best cell made by H-through process b. EQE of the best cell made with the H-through process and of a cell made with the std hydrogenation process c. mobility and carrier concentration of ITO layer after H-through process and after a post-curing without SiN_x:H layer to simulate a standard hydrogenation on wafer substrate insulated by a thick thermal oxide d. absorption of ITO layer after H-through process and after a post-curing without SiN_x:H layer to simulate a standard hydrogenation on glass substrate.

4. Conclusion

In this work, we demonstrated the feasibility of curing sputtering damage and hydrogenating interfacial defects of tunnel-oxide passivating contacts by designing of a SiN_x:H/ITO stack and its thermal treatment. On textured test samples, we show $iV_{OC} > 728$ mV for a 15 nm ITO film capped with SiN_x:H and annealed at 350 °C. Decreasing iV_{OC} for increasing ITO thicknesses is possibly explained by increasingly impeded diffusion of hydrogen through the ITO layer.

Secondly, we observed that R_{sheet} as well as ρ_c of uncapped ITO layers degrade severely for the curing conditions that are needed to recover sputtering damage of our μc-Si(n) contacts, i.e. 30 min at temperatures above 350 °C. The degradation is mitigated by the addition of a SiN_x:H capping layer and by curing in N_2 ambient instead of air. We suppose that the SiN_x:H capping layer prevents the saturation of oxygen vacancies during the subsequent curing that act as dopants in the ITO layer.

Finally, we integrated the developed ITO/SiN_x:H/μc-Si(n) stack as passivating front contacts in solar cells with a hole selective passivating rear contact. The resulting device achieves an efficiency of 22.8% with a V_{OC} close to 720 mV. We measure FF values up to 81.9% with a front contact that uses only 15 nm of ITO. Reducing drastically the amount of ITO is beneficial since indium is a rare material and it will reduce the fabrication costs. Measurements of the EQE suggest parasitic absorption in the near IR-region, associated to an increase of the free carrier concentration in the ITO by the hydrogenation process. Further improvements in cell efficiency are expected by using a TCO with a different response to hydrogenation.

CRediT authorship contribution statement

Frank Meyer: Conceptualization, Methodology, Investigation, Visualization, Writing - original draft, Writing - review & editing. **Arnaud Savoy:** Investigation. **Juan J. Diaz Leon:** Methodology, Investigation. **Marc Persoz:** Investigation. **Xavier Niquille:** Resources. **Christophe Allebé:** Resources. **Sylvain Nicolay:** Project administration. **Franz-Josef Haug:** Project administration, Supervision, Writing - original draft, Writing - review & editing. **Andrea Ingenito:** Conceptualization, Methodology, Supervision, Project administration, Writing - original draft, Writing - review & editing. **Christophe Ballif:** Conceptualization, Methodology, Supervision, Project administration.

Declaration of competing interest

The authors declare that they have no known competing financial interests or personal relationships that could have appeared to influence the work reported in this paper.

Acknowledgments

The authors gratefully acknowledge support by the Swiss Federal Office for Energy through the project “Chess” (Grant No. SI/501253-01) and by the European Commission through the Horizon 2020 project “DISC” (Grant No. 727539).

References

[1] A. Cuevas, Physical model of back line-contact front-junction solar cells, J. Appl. Phys. 113 (2013) 164502, https://doi.org/10.1063/1.4800840.
[2] A. Ingenito, O. Isabella, S. Solntsev, M. Zeman, Accurate opto-electrical modeling of multi-crystalline silicon wafer-based solar cells, Sol. Energy Mater. Sol. Cells 123 (2014) 17–29, https://doi.org/10.1016/j.solmat.2013.12.019.
[3] A. Metz, D. Adler, S. Bagus, H. Blanke, M. Bothar, E. Brouwer, S. Dauwe, K. Dressler, R. Droessler, T. Droste, M. Fiedler, Y. Gassenbauer, T. Grahl, N. Hermert, W. Kuzminski, A. Lachowicz, T. Lauinger, N. Lenck, M. Manole, M. Martini, R. Messmer, C. Meyer, J. Moschner, K. Ramspeck, P. Roth, R. Schönfelder, B. Schum, J. Sticksel, K. Vaas, M. Volk, K. Wangemann, Industrial

high performance crystalline silicon solar cells and modules based on rear surface passivation technology, Sol. Energy Mater. Sol. Cells 120 (2014) 417–425, https://doi.org/10.1016/j.solmat.2013.06.025.
[4] K. Yoshikawa, H. Kawasaki, W. Yoshida, T. Irie, K. Konishi, K. Nakano, T. Uto, D. Adachi, M. Kanematsu, H. Uzu, K. Yamamoto, Silicon heterojunction solar cell with interdigitated back contacts for a photoconversion efficiency over 26%, Nat. Energy. 2 (2017) https://doi.org/10.1038/nenergy.2017.32.
[5] A. Richter, J. Benick, F. Feldmann, A. Fell, M. Hermle, S.W. Glunz, n-Type Si solar cells with passivating electron contact: identifying sources for efficiency limitations by wafer thickness and resistivity variation, Sol. Energy Mater. Sol. Cells 173 (2017) 96–105, https://doi.org/10.1016/j.solmat.2017.05.042.
[6] F. Haase, C. Hollemann, S. Schäfer, A. Merkle, M. Rienäcker, J. Krügener, R. Brendel, R. Peibst, Laser contact openings for local poly-Si-metal contacts enabling 26.1%-efficient POLO-IBC solar cells, Sol. Energy Mater. Sol. Cells 186 (2018) 184–193, https://doi.org/10.1016/j.solmat.2018.06.020.
[7] Y. Tao, V. Upadhyaya, C.-W. Chen, A. Payne, E.L. Chang, A. Upadhyaya, A. Rohatgi, Large area tunnel oxide passivated rear contact n-type Si solar cells with 21.2% efficienc, Prog. Photovoltaics Res. Appl. 24 (2016) 830–835, https://doi.org/10.1002/pip.2793.
[8] U. Römer, R. Peibst, T. Ohrdes, B. Lim, J. Krügener, E. Bugiel, T. Wietler, R. Brendel, Recombination behavior and contact resistance of n+ and p+ poly-crystalline Si/mono-crystalline Si junctions, Sol. Energy Mater. Sol. Cells 131 (2014) 85–91, https://doi.org/10.1016/j.solmat.2014.06.003.
[9] F. Feldmann, M. Bivour, C. Reichel, M. Hermle, S.W. Glunz, Passivated rear contacts for high-efficiency n-type Si solar cells providing high interface passivation quality and excellent transport characteristics, Sol. Energy Mater. Sol. Cells 120 (2014) 270–274, https://doi.org/10.1016/j.solmat.2013.09.017.
[10] J. Stuckelberger, G. Nogay, P. Wyss, Q. Jeangros, C. Allebé, F. Debrot, X. Niquille, M. Ledinsky, A. Fejfar, M. Despeisse, F.J. Haug, P. Löper, C. Ballif, Passivating electron contact based on highly crystalline nanostructured silicon oxide layers for silicon solar cells, Sol. Energy Mater. Sol. Cells 158 (2016) 2–10, https://doi.org/10.1016/j.solmat.2016.06.040.
[11] G. Yang, A. Ingenito, N. Van Hameren, O. Isabella, M. Zeman, Design and application of ion-implanted polySi passivating contacts for interdigitated back contact c-Si solar cells, Appl. Phys. Lett. 108 (2016), https://doi.org/10.1063/1.4940364.
[12] A. Ingenito, G. Nogay, J. Stuckelberger, P. Wyss, L. Gnocchi, C. Alleb, M. Despeisse, F. Haug, L. Philipp, C. Ballif, Phosphorous-doped silicon carbide as front-side full-area passivating contact for double-side contacted c-Si solar cells, 1-9, https://doi.org/10.1109/JPHOTOV.2018.2886234, 2018.
[13] G. Nogay, A. Ingenito, E. Rucavado, Q. Jeangros, J. Stuckelberger, P. Wyss, C. Ballif, M. Morales-masis, F. Haug, L. Philipp, Crystalline silicon solar cells with coannealed electron- and hole-selective SiC x passivating contacts, IEEE J. Photovoltaics (2018) 1–8, https://doi.org/10.1109/JPHOTOV.2018.2866189.
[14] J. Stuckelberger, G. Nogay, P. Wyss, A. Ingenito, C. Allebé, J. Horzel, B.A. Kamino, M. Despeisse, F.-J. Haug, P. Löper, Recombination analysis of phosphorus-doped nanostructured silicon oxide passivating electron contacts for silicon solar cells, IEEE J. Photovoltaics 8 (2018) 389–396.
[15] R. Peibst, Y. Larionova, S. Reiter, T.F. Wietler, N. Orlowski, H. Mehlich, B. Min, M. Stratmann, D. Tetzlaff, J. Kr, S. Frigge, R. Brendel, Building blocks for industrial , screen-printed double-side contacted POLO cells with highly transparent ZnO : Al layers, IEEE J. Photovoltaics (2018) 1–7, https://doi.org/10.1109/JPHOTOV.2018.2813427.
[16] A. Stesmans, Dissociation kinetics of hydrogen-passivated defects at the interface, Phys. Rev. B Condens. Matter 61 (2000) 8393–8403, https://doi.org/10.1103/PhysRevB.61.8393.
[17] A.G. Aberle, Surface passivation of crystalline silicon solar cells: a review, Prog. Photovoltaics Res. Appl. 8 (2000) 473–487, https://doi.org/10.1002/1099-159X(200009/10)8:5<473::AID-PIP337>3.0.CO;2-D.
[18] B. Hallam, D. Chen, M. Kim, B. Stefani, B. Hoex, M. Abbott, S. Wenham, The role of hydrogenation and gettering in enhancing the efficiency of next-generation Si solar cells: an industrial perspective, Phys. Status Solidi Appl. Mater. Sci. 214 (2017), https://doi.org/10.1002/pssa.201700305.
[19] M. Lehmann, N. Valle, J. Horzel, A. Pshenova, P. Wyss, M. Döbeli, M. Despeisse, S. Eswara, T. Wirtz, Q. Jeangros, A. Hessler-wyser, F. Haug, A. Ingenito, C. Ballif, E. Polytechnique, F. De Lausanne, M. Imt, T. Film, R.D. La Maladière, Solar Energy Materials and Solar Cells Analysis of hydrogen distribution and migration in fired passivating contacts, Sol. Energy Mater. Sol. Cells 200 (2019) 110018, https://doi.org/10.1016/j.solmat.2019.110018.
[20] D. Chen, Y. Chen, Z. Wang, J. Gong, C. Liu, Y. Zou, Y. He, Y. Wang, L. Yuan, W. Lin, R. Xia, L. Yin, X. Zhang, G. Xu, Y. Yang, H. Shen, Z. Feng, P.P. Altermatt, P. J. Verlinden, 24.58% total area efficiency of screen-printed, large area industrial silicon solar cells with the tunnel oxide passivated contacts (i-TOPCon) design, Sol. Energy Mater. Sol. Cells 206 (2020) 1–8, https://doi.org/10.1016/j.solmat.2019.110258.
[21] A. Ingenito, G. Limodio, P. Procel, G. Yang, H. Dijkslag, O. Isabella, M. Zeman, Silicon solar cell architecture with front selective and rear full area ion-implanted passivating contacts, 1700040,4-9, https://doi.org/10.1002/solr.201700040, 2017.
[22] C. Messmer, M. Bivour, C. Luderer, L. Tutsch, J. Schön, M. Hermle, Influence of interfacial oxides at TCO/doped Si thin film contacts on the charge carrier, Transport of Passivating Contacts 10 (2020) 343–350.
[23] F. Feldmann, K.U. Ritzau, M. Bivour, A. Moldovan, S. Modi, J. Temmler, M. Hermle, S.W. Glunz, High and low work function materials for passivated contacts, Energy Procedia 77 (2015) 263–270, https://doi.org/10.1016/j.egypro.2015.07.037.
[24] A. Moldovan, F. Feldmann, K. Kaufmann, S. Richter, M. Werner, C. Hagendorf, M. Zimmer, J. Rentsch, M. Hermle, Tunnel oxide passivated carrier-selective contacts based on ultra-thin SiO2 layers grown by photo-oxidation or wet-chemical oxidation in ozonized water, 2015, IEEE 42nd Photovolt. Spec. Conf. PVSC 2015 (2015), https://doi.org/10.1109/PVSC.2015.7356144.
[25] A. Fukano, H. Oyanagi, Highly insulating ultrathin SiO2 film grown by photooxidation, J. Appl. Phys. 94 (2003) 3345–3349, https://doi.org/10.1063/1.1597940.
[26] A. Moldovan, F. Feldmann, G. Krugel, M. Zimmer, J. Rentsch, M. Hermle, A. Roth-Fölsch, K. Kaufmann, C. Hagendorf, Simple cleaning and conditioning of silicon surfaces with UV/ozone Sources, Energy Procedia 55 (2014) 834–844, https://doi.org/10.1016/j.egypro.2014.08.067.
[27] D.M. Kane, R.M. Swanson, Measurement of the emitter saturation current by a contactless photoconductivity decay method, in: Proc. 18th IEEE Photovolt. Spec. Conf., 1985, pp. 578–583.
[28] R.A. Sinton, A. Cuevas, M. Stuckings, Quasi-steady-state photoconductance, a new method for solar cell material and device characterization, Conf. Rec. Twenty Fifth IEEE Photovolt. Spec. Conf. - (1996) 457–460.
[29] A. Cuevas, R.A. Sinton, Prediction of the open-circuit voltage of solar cells from the steady-state photoconductance, Prog. Photovoltaics Res. Appl. 5 (1997) 79–90, https://doi.org/10.1002/(SICI)1099-159X(199703/04)5:2<79::AID-PIP155>3.0.CO;2-J.
[30] H.H. Berger, Contact resistance and contact resistivity, J. Electrochem. Soc. 119 (1972) 507–514, https://doi.org/10.1149/1.2404240.
[31] G.K. Reeves, H.B. Harrison, Obtaining the specific contact resistance from transmission line model measurements, IEEE Electron. Device Lett. 3 (1982) 111–113, https://doi.org/10.1109/EDL.1982.25502.
[32] S.M. Sze, L.J. van der PAUW, A method of measuring specific resistivity and Hall effect of discs of arbitrary shape, in: Semicond. Devices Pioneer. Pap., WORLD SCIENTIFIC, 1991, pp. 174–182, https://doi.org/10.1142/9789814503464_0017.
[33] F.J. Haug, A. Ingenito, F. Meyer, S. Libraro, N. Bolis, J.J.D. Leon, C. Allebe, C. Ballif, Contributions to the contact resistivity in fired tunnel-oxide passivating contacts for crystalline silicon solar cells, IEEE J. Photovoltaics. 9 (2019) 1548–1553, https://doi.org/10.1109/JPHOTOV.2019.2939880.